Letter Vol. 6, No. 8 / August 2019 / Optica 1046

optica

Analytical description of a luminescent solar concentrator

Ilya Sychugov

Department of Applied Physics, School of Engineering Sciences, KTH-Royal Institute of Technology, 16440 Stockholm, Sweden (ilyas@kth.se)

Received 20 March 2019; revised 22 May 2019; accepted 21 June 2019 (Doc. ID 362951); published 13 August 2019

A luminescent solar concentrator focuses solar light spectrally and spatially to convert it to electricity. Due to a large number of input parameters and their complex effect on the device efficiency, it is typically described by numerical simulations. Here, an analytical solution is presented, which significantly reduces the complexity of the optical efficiency evaluation. The equations were derived using probabilistic approach and validated by simulations. The implementation by a computer algebra program yields instant results for any set of input parameters. It allows a higher level of analysis, where an inverse task of finding parameters for a given efficiency can be readily solved. The obtained explicit expressions provide a clear standard for theoretical description of such devices.

https://doi.org/10.1364/OPTICA.6.001046

Radiation conversion by luminescence concentration was considered decades ago, mainly motivated by detector size reduction [1–3]. Acrylic glasses filled with organic dyes were proposed to convert incoming light to fluorescence for subsequent detection by small semiconductor photodetectors [4,5]. With the development of detector technology and due to inherent limitations of the available fluorophores, this method did not gain much traction. Recently, stimulated by advances in colloidal quantum dot synthesis, it has regained attention [6,7].

The operation principle of a luminescent solar concentrator (LSC) is based on a total internal reflection of the re-emitted light for large angles, which is waveguided to the edges for conversion to electricity [8,9]. For this purpose, a glass (plastic) slab is enriched with fluorophores, and photovoltaic cells are attached to the slab perimeter (Fig. 1). For such a device the power conversion efficiency is a key parameter. Multiple loss mechanisms, however, exist in the system. The re-emitted light can be absorbed by the matrix material, by fluorophores, or it can be scattered out of the slab. The apparent complexity leads to the use of numerical simulations for the efficiency estimations [10–12].

Analytical treatment can substantially reduce the complexity of the problem in the sense of a classical definition of complexity as the minimal length of a "code" needed to attain a result [13]. In addition to reduced computational times, explicit expressions facilitate a unified benchmark tool, as opposite to long, undisclosed user-dependent codes. Finally, expedient results from a computer algebra program would imply the possibility of a higher level of analysis, such as solving an inverse problem of determining device parameters for a desired output efficiency.

Here, an analytical solution has been derived by probabilistic treatment, including all the main loss mechanisms. It was based on the obtained distribution of the optical path lengths for an isotropic emitter, randomly placed in a rectangular slab with absorbing edges. In this framework, a result can be obtained instantly by a computer algebra program as a continuous function of input parameters. Obtained values compare well with numerical simulations and represent a transparent and direct method for the complete analysis of LSC performance.

We start by considering an isotropic emitter randomly placed inside a rectangular slab (height h, width w, and diagonal d) (Fig. 1). Isotropic emission corresponds to the light output pattern of quantum dots (QDs), which are typically spherical without specific dipole orientation [14]. For organic dyes, this condition reflects a random orientation of the molecules uniformly distributed in the slab. It can be shown that in the plane of the slab (Fig. 1, left), the properly normalized probability density function (PDF) for a photon to travel an optical path r is a piece-wise function (see Section S1A in Supplement 1 for the derivation):

$$p(r) = \begin{cases} \dfrac{2w + 2h - 2r}{\pi h w}, & 0 < r < w \\ \dfrac{2r - 2\sqrt{r^2 - w^2}}{\pi w r}, & w < r < h. \\ \dfrac{2r^2 - 2h\sqrt{r^2 - w^2} - 2w\sqrt{r^2 - h^2}}{\pi h w r}, & h < r < d \end{cases} \quad (1)$$

This distribution is shown in Fig. 2 for two different geometries (blue and red lines). Points are the results of numerical simulations, where isotropic emitters were placed all over the slab, and the frequency for a million of optical paths was calculated. Numerical solutions indeed converge to the analytical formula $p(r)$.

Next, we note that together with the in-plane distribution, there is a spread of optical paths in the plane perpendicular to the slab, as shown in Fig. 1, right (slab thickness Δ). Here photons emitted along two directions are shown, undergoing total internal reflection until the edge. Photons emitted to the escape cone (within the critical angle α_c) directly contribute to the losses. For the typical refraction index of glass (polymers) $n = 1.5$, the critical angle is $\alpha_c \approx 42°$. It is clear that the slab thickness plays no role in the out-of-plane optical path distribution. Regardless of

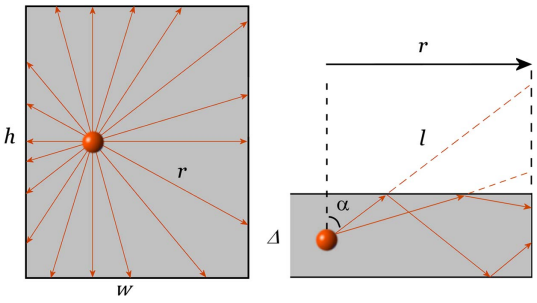

Fig. 1. Total optical path distribution from isotropic emitters in a rectangular slab (height h, width w, and thickness Δ) stems from in-plane $p(r)$ and out-of-plane $q_r(l)$ distributions.

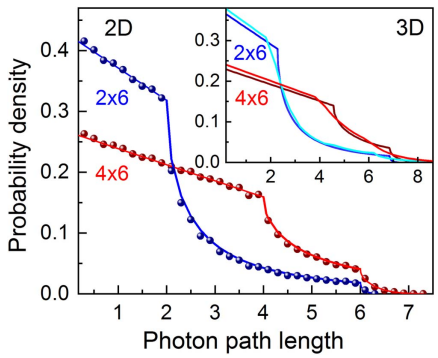

Fig. 2. Distribution $p(r)$ of the optical path lengths for the photons from an isotropic emitter randomly placed in a 2D slab. Data points are simulated, and the lines are from Eq. (1) ($h = 6$ and $w = 4$ or two length units). The inset shows full 3D distribution $q(l)$: bright lines are the exact solutions, and dark lines are the approximate solutions from Eq. (2).

the first point of the total internal reflection (slab thickness), the optical path length (red dashed) depends only on the angle α.

For the out-of-plane distribution, the distribution for an isotropic emitter is (see Supplement 1, S1B)

$$q_r(l) = \frac{1}{2\pi} \cdot \frac{r}{l\sqrt{l^2 - r^2}},$$

for a given in-plane optical path length to the edge r. Convoluting both distributions, one can obtain an expression for the full distribution of optical path lengths for the 3D case:

$$q(l) = \frac{1}{2\pi l} \int_{\frac{2}{3}l}^{l} \frac{p(r')r'}{\sqrt{l^2 - r'^2}} \mathrm{d}r'.$$

Integration limits come from the escape cone, where $r < l < nr = 3r/2$ (see Supplement 1, S1C). This integral can be solved analytically using special functions; exact solutions are in Supplement 1, S1C and are presented graphically in Fig. 2, inset, as bright blue and red lines. It is seen that the distributions are smoothened and stretched to slightly longer values as compared to the 2D case. The solutions were again validated by simulations, and numerical results converge to the analytical expressions (Fig. S1). While the exact formulas are possible to obtain, the extensive presence of special functions make them not very practical. To simplify the result to elementary functions, one can note that the out-of-plane distribution $q_r(l)$ does not deviate far from the distance to the edge r due to the limits set by the escape cone. Thus, the average value $\langle l \rangle$ can be taken instead of the distribution $q_r(l)$. It can be written as $l \approx \langle l \rangle = k \cdot r$ (see Supplement 1, S1B), where

$$k \approx 1.14.$$

Then the approximate solution for the 3D case can be represented simply through the 2D solution (see Supplement 1, S2A):

$$q(l) \approx p(l/k).$$

A properly normalized PDF then can be written *explicitly* as

$$q(l) = \begin{cases} \dfrac{2w + 2h - 2l/k}{\pi hwk}, & 0 < l < kw \\ \dfrac{2l - 2\sqrt{l^2 - (kw)^2}}{\pi lwk}, & kw < l < kh. \\ \dfrac{2l^2/k - 2h\sqrt{l^2 - (kw)^2} - 2w\sqrt{l^2 - (kh)^2}}{\pi lhwk} & kh < l < kd \end{cases} \tag{2}$$

This function is shown in Fig. 2, inset, as dark blue and red lines. It reveals that the approximate solutions nearly coincide with the exact ones, indicating only a minor influence from the introduced assumption. The practical meaning of $q(l)$ is that the probability for a photon from an isotropic emitter randomly placed in the slab to experience an optical path $(l; l + dl)$ would be $q(l)dl$.

From Eq. (2), one can already get some insight into the effect of the slab geometry. The probability of having an optical path below the slab width (aspect ratio $\beta = w/h$) can be calculated as $P_w \approx 0.31\beta + 0.56$ (see Supplement 1, Section S2B). It becomes clear that the rectangle width w limits most of the photon paths (Fig. S1, inset). For example, for the slab with a "golden ratio" $\beta \approx 0.62$, often used in architectural design of windows, ~75% of photons will travel distances shorter than w.

With the optical path-length distribution established, the effect of matrix absorption on device efficiency can be readily evaluated. Let the linear absorption coefficient of the matrix be α [cm^{-1}]. The probability of reaching the edge for a photon travelling distance l' is $\exp(-\alpha l')$, i.e., a random process with an average rate α. Then the total probability of reaching the edge is

$$f(\alpha) = \int_0^{l\,\max} q(l') \cdot \exp(-\alpha l') \mathrm{d}l',$$

where $l_{\max} = kd$. Calculating this integral yields (Supplement 1, S3)

$$f(\alpha) = \frac{2}{\alpha^2 hw\pi k^2}((h + w)\alpha k - (kd\alpha + 1) \cdot e^{-kd\alpha} + e^{-kh\alpha} + e^{-kw\alpha} - 1) - \Im_1 - \Im_2, \tag{3}$$

where two integrals are

$$\Im_1 = \frac{2}{w\pi k} \int_{kw}^{kd} \frac{\sqrt{l^2 - (kw)^2}}{l} \exp(-\alpha l) \mathrm{d}l, \tag{3a}$$

$$\Im_2 = \frac{2}{h\pi k} \int_{kh}^{kd} \frac{\sqrt{l^2 - (kh)^2}}{l} \exp(-\alpha l) \mathrm{d}l. \tag{3b}$$

Formula (3) gives instant results for the effect of matrix absorption on the efficiency for a rectangular slab of any geometry and absorption coefficient, using an algebra program on a desktop computer (Fig. 3, left). One can compare the results with existing Monte–Carlo simulations using, e.g., results from [10] for PMMA ($\alpha_{\mathrm{PMMA}} = 0.03$ cm^{-1}, blue dots) and for soda-lime glass

($\alpha_{WG} = 0.5$ cm^{-1}, red dots) in a square slab. Thus, analytical results of Eq. (3) coincide reasonably well with numerical simulations. The limitations of numerical Monte–Carlo method also become obvious: only one data point can be obtained per run, and the proper convergence needs to be verified. The analytical result [Eq. (3)], in contrast, produces a full functional dependence at once, and changing geometry is just a matter of entering new values.

Separately from the matrix-induced losses, the fluorophores themselves may attenuate re-emitted light. Consider first the effect of scattering. Let the linear scattering coefficient be α_{sc}[cm^{-1}]. It can be expressed via QD scattering cross-section σ_{sc}, and their concentration N as $\alpha_{sc} = \sigma_{sc}N$. We invoke the Rayleigh scattering on particles smaller than the wavelength, which is nearly isotropic. The probability of not being scattered after travelling the distance l' is $\exp(-\alpha_{sc}l')$. These photons will contribute to the total optical efficiency similarly to the absorption case:

$$\chi_0(\alpha_{sc}) = f(\alpha_{sc}).$$

In addition, there will be photons, which underwent a scattering event to the waveguiding mode. The probability of being scattered within a distance l' is $1 - \exp(-\alpha_{sc}l')$. Let δ be the probability of scattering to the waveguided mode and not to the escape cone ($\delta \approx 75\%$ for $n = 1.5$, see Supplement 1, S4). Then the probability to reach the edge after one scattering event (see Supplement 1, S5 for derivations) is

$$\chi_1(\alpha_{sc}) = \delta \cdot (1 - f(\alpha_{sc})) \cdot f(\alpha_{sc}).$$

Summing up all contributions from multiple scattering events and using geometrical series one obtains

$$\chi(\alpha_{sc}) = \sum_{i=0}^{\infty} \chi_i(\alpha_{sc}) = \frac{f(\alpha_{sc})}{1 - \delta \cdot (1 - f(\alpha_{sc}))}.$$

One can quickly evaluate that for $\delta = 1$ (scattering without losses), the total probability is unity. For $\delta = 0$ (scattering as a full loss), the expression becomes the same as for the absorption case. Also if the scattering coefficient $\alpha_{sc} = 0$, the optical efficiency is unity. An assumption of the Markov process was made here, so that the same optical path-length distribution $q(l)$ could be used after every scattering event.

Similarly to the scattering loss, the fluorophores can re-absorb propagating light with subsequent re-emission. Let the linear reabsorption coefficient be α_{re} [cm^{-1}]. Introducing a nanocrystal reabsorption cross-section σ_{re}, it can be written as $\alpha_{re} = \sigma_{re}N$. If this process dominates the losses (no scattering or matrix absorption), it can be evaluated similar to the scattering as

$$\xi(\alpha_{re}) = \frac{f(\alpha_{re})}{1 - \delta \cdot \mathrm{QY} \cdot (1 - f(\alpha_{re}))}, \quad (4)$$

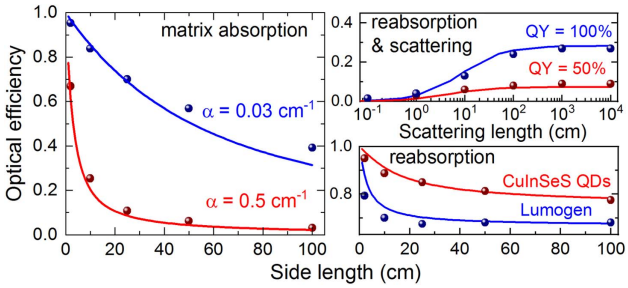

Fig. 3. Comparison of analytical solutions [Eqs. (3)–(5)] for different loss mechanisms (lines) with numerical simulations (points) from [10,11].

where QY is the quantum yield (QY ≤ 1). Here losses after every reabsorption event come not only from the escape cone, but also from the imperfect light conversion of emitters. An additional complication is a spectral dependence of the reabsorption coefficient $\alpha_{re} = \alpha_{re}(\lambda)$, due to a wavelength-dependent overlap of the luminophore emission and absorption bands. A spectral convolution can be used in this case with a properly normalized luminophore emission spectrum $I(\lambda)$:

$$\xi = \int_{\lambda\,\mathrm{min}}^{\lambda\,\mathrm{max}} I(\lambda) \cdot \xi(\alpha_{re}(\lambda))\mathrm{d}\lambda.$$

As a first approximation, two reabsorption coefficients for the regions with strong and weak overlaps of the absorption/emission spectra can be introduced. For example, for Lumogen [10] a third of the emission band can be set as $\alpha_{re1} = 1.5$ cm^{-1}, while the rest is nearly reabsorption free: $\alpha_{re2} = 0$. The total optical efficiency in this case becomes a weighted sum $\xi(\alpha_{re1})/3 + 2/3$. Similarly for CuInSeS QDs [10], a quarter of the band has $\alpha_{re3} = 0.3$ cm^{-1}, and for the rest $\alpha_{re4} = 0$, corresponding to the total efficiency $\xi(\alpha_{re3})/4 + 3/4$. In Fig. 3, right bottom, analytical results for these luminophores are shown. Even without a proper spectral convolution, they reveal main features from the numerical Monte–Carlo simulations (dots).

So far, we considered scenarios where a single loss mechanism dominates. In practice, they all can co-exist, and their simultaneous contribution should be taken into account. Using similar combinatorics arguments as above (see Supplement 1, S6), it can be shown that for the case of scattering and reabsorption co-existence, the optical efficiency becomes

$$\varphi(\alpha_{sc}, \alpha_{re}) = \frac{f(\alpha_{sc} + \alpha_{re})}{1 - \frac{\delta \cdot \alpha_{sc} + \delta \cdot \mathrm{QY} \cdot \alpha_{re}}{\alpha_{sc} + \alpha_{re}} (1 - f(\alpha_{sc} + \alpha_{re}))}. \quad (5)$$

To validate this derivation and result, a comparison with numerical Monte–Carlo simulations from [11] is shown in Fig. 3, right top. Here, the optical efficiency as a function of the scattering length ($l_{sc} = 1/\alpha_{sc}$) is presented for Si QDs with a QY of 50% (red) and 100% (blue) for a square slab 1×1 m^2 using $\alpha_{re} = 0.08$ cm^{-1}. For this type of fluorophore, the wavelength dependence of the reabsorption within the emission band is small due to a very large Stokes shift [15,16]. As in the numerical Monte–Carlo simulations [11], here the optical efficiency including the first absorption event is shown, i.e., $\delta \cdot \mathrm{QY} \cdot \varphi(\alpha_{sc}, \alpha_{re})$. Again, the agreement with numerical Monte–Carlo simulations is reasonable. Combining all loss mechanisms, a general solution is

$$g(\alpha_{sc}, \alpha_{re}, \alpha) = \frac{f(\alpha_{sc} + \alpha_{re} + \alpha)}{1 - \frac{\delta \cdot \alpha_{sc} + \delta \cdot \mathrm{QY} \cdot \alpha_{re}}{\alpha_{sc} + \alpha_{re} + \alpha} (1 - f(\alpha_{sc} + \alpha_{re} + \alpha))}. \quad (6)$$

So Eqs. (3) and (6) fully describe the effect of propagation losses in an LSC device. Input parameters are scattering (α_{sc}); reabsorption (α_{re}); and matrix absorption (α) coefficients; geometry of the rectangular slab, height and width (h, w); fraction of the emission to the waveguiding mode δ ($\delta = 75\%$ for $n = 1.5$); fluorophore quantum yield (QY); and the correction factor for 3D geometry $k \approx 1.14$. These formulas can replace Monte–Carlo calculations and provide a quick and transparent tool for a thorough device analysis. Below, we show their application for optimization of a particular configuration. The optical power output of the device $\gamma[W]$, as collected at the edges, is

$$\gamma = \Phi \cdot h \cdot w \cdot (1 - T) \cdot \delta \cdot \mathrm{QY} \cdot \eta \cdot g(\alpha_{sc}, \alpha_{re}, \alpha), \quad (7)$$

where Φ is the incoming energy flux [W/cm^2], T is a transmitted fraction of the incoming sunlight ($1 - T$ is the absorbed fraction), and $\eta = \epsilon_{PL}/\epsilon_{\text{sun}}$ is the energy conversion coefficient of the luminescence, defined as the ratio of luminescence and solar peak position energies. Product $\delta \cdot \text{QY}$ signifies losses after the first absorption event, i.e., before the waveguiding mode is initiated. Transmission of the visible light through the device is thickness (Δ) dependent $T = \exp(-\alpha_{\text{vis}}\Delta)$, where $\alpha_{\text{vis}} = \sigma_{\text{vis}}N$ is the average linear absorption coefficient of the fluorophore in the visible range, N is a fluorophore concentration, and σ_{vis} is the average absorption cross section (reflection neglected). This effectively gives three more input parameters: η, Δ, and σ_{vis}. If necessary, spectral dependence of the reabsorption coefficient can be included by convolution with the normalized emission spectrum $I(\lambda)$. So considering δ, k, and Φ as constants, in total there are 11 independent input parameters, where at least three in general have wavelength dependence: $I(\lambda), \alpha_{re}(\lambda)$, and $\sigma_{\text{vis}}(\lambda)$.

An example for Si QDs, often used for this application [11,16,17], is shown in Fig. 4, top. For these QDs, the energy conversion factor can be set $\eta \approx 0.6$ for the average solar photon energy of 2.5 eV and the luminescence peak at 1.5 eV. Other parameters are reabsorption and scattering coefficients: $\alpha_{re} = 0.03$ cm^{-1} [16] and $\alpha_{sc} = 0.001$ cm^{-1} [11] for 0.1 wt.% concentration (5 nm diameter QDs). The solar influx is $\Phi = 0.1$ W/cm^2, and the transmission T is set to 75%. A square slab ($h = w$) made of PMMA ($\alpha = 0.03$ cm^{-1}) is considered. Results compare very well with experimental data (star) and numerical simulations (dots) for Si QDs with QY = 46% [16]. A file generating such curves in MAPLE is given in Dataset 1, Ref. [18].

A practical question for LSCs with Si QD laminates is which type of glass can be used for efficient operation in building-integrated photovoltaics. Rectangular slab geometry is more relevant here (aspect ratio $\beta = w/h$). Several optical power curves for different matrix absorption coefficients are plotted for $h = 100$ cm in Fig. 4, left (QY = 1). In the absence of all propagation-related losses, i.e., $g(\alpha_{sc}, \alpha_{re}, \alpha) = 1$, the optical power conversion efficiency equals $(1 - T)\delta\eta = 22.5\%$ for $T = 0.5$ (top dashed line). We can also set a minimum acceptable threshold for the power conversion to 7% (lower dashed line). This roughly corresponds to 5% (50 W/m^2 electrical power output), taking into account conversion losses at the last stage, such as the PV cell efficiency. The grey area in between these lines then shows an acceptable working range. As expected, the deviation from the loss-free case is growing with an increasing aspect ratio and stronger matrix absorption. A larger device area does not improve the output power after a certain point, where propagation losses start dominating.

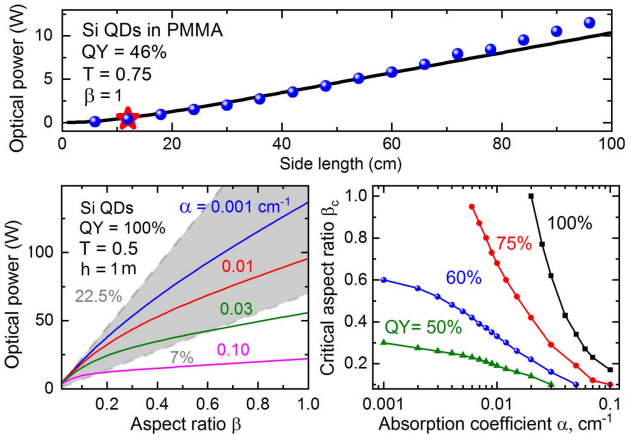

Fig. 4. (top and left) Device power output (line) from the analytical solution of Eq. (7). The star and dots are experimental data and numerical simulations from [16]. (right) Critical aspect ratio β_c, resulting in 7% efficiency, for different quantum yields and absorption coefficients.

From such a plot, one can graphically solve an inverse problem of finding input parameters for a given threshold efficiency. In Fig. 4, right, the critical aspect ratio β_c corresponding to a 7% efficiency is shown as a function of α for different QY values. It is seen that for the golden ratio slab $\beta_c \approx 0.62$ and QY = 60%, a very low matrix absorption coefficient needed $\alpha = 10^{-3}$ cm^{-1}, as in N-BK7 glass. Increasing QY by only 15% relaxes this condition by an order of magnitude, making more affordable white soda lime glass ($\alpha \approx 0.03$ cm^{-1}) a viable option.

In conclusion, analytical formulas were derived to account for different losses in a luminescent solar concentrator. The results were validated by numerical simulations of optical path distribution and propagation losses. The obtained solutions can be used to quickly evaluate the LSC performance for different compositions and designs [19–22], as well as for the description of light propagation in solar-pumped lasers [23] and similar systems.

Funding. Swedish Energy Agency (46360-1).

See Supplement 1 for supporting content.

REFERENCES

1. G. Keil, J. Appl. Phys. **40**, 3544 (1969).
2. J. S. Batchelder, A. H. Zewail, and T. Cole, Appl. Opt. **18**, 3090 (1979).
3. E. Yablonovitch, J. Opt. Soc. Am. **70**, 1362 (1980).
4. W. H. Weber and J. Lambe, Appl. Opt. **15**, 2299 (1976).
5. A. Goetzberger and W. Greubel, Appl. Phys. **14**, 123 (1977).
6. F. Purcell-Milton and Y. K. Gun'ko, J. Mater. Chem. **22**, 16687 (2012).
7. W. G. J. H. M. van Sark, Renew. Energy **49**, 207 (2013).
8. C. S. Erickson, L. R. Bradshaw, S. McDowall, J. D. Gilbertson, D. R. Gamelin, and D. L. Patrick, ACS Nano **8**, 3461 (2014).
9. H. B. Li, K. Wu, J. Lim, H. Song, and V. I. Klimov, Nat. Energy **1**, 16157 (2016).
10. F. Meinardi, F. Bruni, and S. Brovelli, Nat. Rev. Mater. **2**, 17072 (2017).
11. S. K. E. Hill, R. Connell, C. Peterson, J. Hollinger, M. A. Hillmyer, U. Kortshagen, and V. E. Ferry, ACS Photon. **6**, 170 (2019).
12. X. M. Hu, R. D. Kang, Y. Y. Zhang, L. G. Deng, H. Z. Zhong, B. S. Zou, and L. J. Shi, Opt. Express **23**, A858 (2015).
13. A. N. Kolmogorov, Probl. Inf. Transm. **1**, 3 (1965).
14. T. Schmidt, A. I. Chizhik, A. M. Chizhik, K. Potrick, A. J. Meixner, and F. Huisken, Phys. Rev. B **86**, 125302 (2012).
15. I. Sychugov, F. Pevere, J. W. Luo, A. Zunger, and J. Linnros, Phys. Rev. B **93**, 161413 (2016).
16. F. Meinardi, S. Ehrenberg, L. Dhamo, F. Carulli, M. Mauri, F. Bruni, R. Simonutti, U. Kortshagen, and S. Brovelli, Nat. Photonics **11**, 177 (2017).
17. A. Marinins, R. Shafagh, W. Van der Wijngaart, T. Haraldsson, J. Linnros, J. G. C. Veinot, S. Popov, and I. Sychugov, ACS Appl. Mater. Interfaces **9**, 30267 (2017).
18. Maple file with formulas, https://doi.org/10.6084/m9.figshare.7868843.
19. F. Meinardi, Q. A. Akkerman, F. Bruni, S. Park, M. Mauri, Z. Y. Dang, L. Manna, and S. Brovelli, ACS Energy Lett. **2**, 2368 (2017).
20. R. Sumner, S. Eiselt, T. B. Kilburn, C. Erickson, B. Carlson, D. R. Gamelin, S. McDowall, and D. L. Patrick, J. Phys. Chem. C **121**, 3252 (2017).
21. M. R. Bergren, N. S. Makarov, K. Ramasamy, A. Jackson, R. Guglielmetti, and H. McDaniel, ACS Energy Lett. **3**, 520 (2018).
22. I. Papakonstantinou and C. Tummeltshammer, Optica **2**, 841 (2015).
23. S. Nechayev, P. D. Reusswig, M. A. Baldo, and C. Rotschild, Sci. Rep. **6**, 38576 (2016).

optica

Analytical description of a luminescent solar concentrator device: supplementary material

ILYA SYCHUGOV

Department of Applied Physics, School of Engineering Sciences, KTH-Royal Institute of Technology, Stockholm, Sweden
ilyas@kth.se

Published 13 August 2019

This document provides supplementary information to "Analytical description of a luminescent solar concentrator device," https://doi.org/10.1364/OPTICA.6.001046. Here detailed analytical derivations are provided together with additional verification simulations.

Section S1. Derivation of the optical path length distribution in a slab.

We are interested in the probability density for a photon to travel distance r to the edge of a rectangular slab for an isotropic point-like source randomly placed inside it.

A) 2D case in-plane (XY plane).

Consider edge element of a length dy. The fraction of the isotropic emission from a point source at distance r into the edge element dy:

$$f = \frac{d\varphi}{2\pi}$$

From the yellow triangle:

$$dy \cdot sin(\pi - \theta) = 2 \cdot (r - dy \cdot cos(\pi - \theta)) \cdot sin(d\varphi/2)$$

For small φ one can approximate $\sin(d\varphi/2) \approx d\varphi/2$. For small dy one can simplify $(r - dy \cdot \cos(\pi - \theta)) \approx r$. Then

$$dy \cdot sin(\theta) \approx r \cdot d\varphi$$

Then the fraction f for a single source becomes:

$$f = \frac{dy \cdot sin(\theta)}{2\pi r}$$

Elementary length ds of the arc with radius r contributing to the signal for the angle θ (blue segment):

$$ds = \frac{d\theta}{2\pi} \cdot 2\pi r = r d\theta$$

If the arc is limited by angles $\theta_{1,2}$ the total fraction of photons from the arc of a length s, arriving to the element dy (summing up signal from all the sources at a distance r):

$$F = \int_0^s f ds = \frac{dy}{2\pi}\int_{\theta_1}^{\theta_2} sin(\theta)\, d\theta = \frac{dy}{2\pi}(cos(\theta_1) - cos(\theta_2))$$

Finally, for the total fraction of photons reaching the edge (length h) after travelling distance r one should integrate over the whole edge length:

$$p(r) = \frac{1}{2\pi}\int_0^h (cos(\theta_1) - cos(\theta_2))\, dy$$

which, after normalization, represents the probability density function. Since limiting angles $\theta_{1,2}$ vary depending on the geometry and the exact position of dy several cases should be considered. For certainty a rectangular with a width smaller than the height ($w < h$) is taken into account.

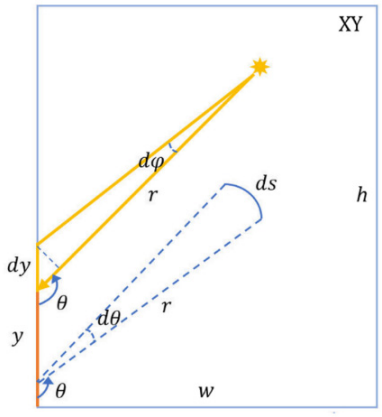

Scheme S1. Notations used in the derivation of the section S1A.

A1) For $r < \frac{h}{2}$:
Three different cases can be considered:
1. For $0 < y < r$ the arc is from θ_1 to π, where $\cos(\theta_1) = \frac{y}{r}$
2. For $r < y < h - r$ the arc is from 0 to π
3. For $h - r < y < h$ the arc is from 0 to θ_2, where $\cos(\pi - \theta_2) = \frac{h-y}{r}$, $\cos(\theta_2) = -\frac{h-y}{r}$

And the total number of photons can be calculated by integrating respective parts:

$$\boldsymbol{p_{left1}(r) = \frac{1}{2\pi}\left(\int_0^r \left(\frac{y}{r}+1\right)dy + \int_r^{h-r} 2dy + \int_{h-r}^{h}\left(1+\frac{h-y}{r}\right)dy\right) = \frac{2h-r}{2\pi}}$$

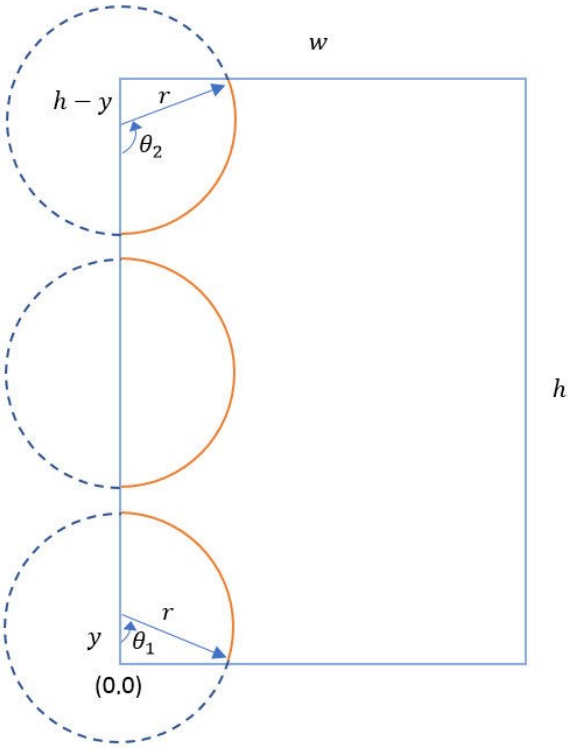

Scheme S2. Notations used in the derivation of the section S1A1.

A2) For $\frac{h}{2} < r < w$
Again three different cases can be considered:
1. For $0 < y < h - r$ the arc is from θ_1 to π
2. For $h - r < y < r$ the arc is from θ_1 to θ_2
3. For $r < y < h$ the arc is from 0 to θ_2

$$\boldsymbol{p_{left2}(r) = \frac{1}{2\pi}\left(\int_0^{h-r}\left(\frac{y}{r}+1\right)dy + \int_{h-r}^{r}\left(\frac{y}{r}+\frac{h-y}{r}\right)dy + \int_r^{h}\left(1+\frac{h-y}{r}\right)dy\right) = \frac{2h-r}{2\pi}}$$

The same result as for the case above.

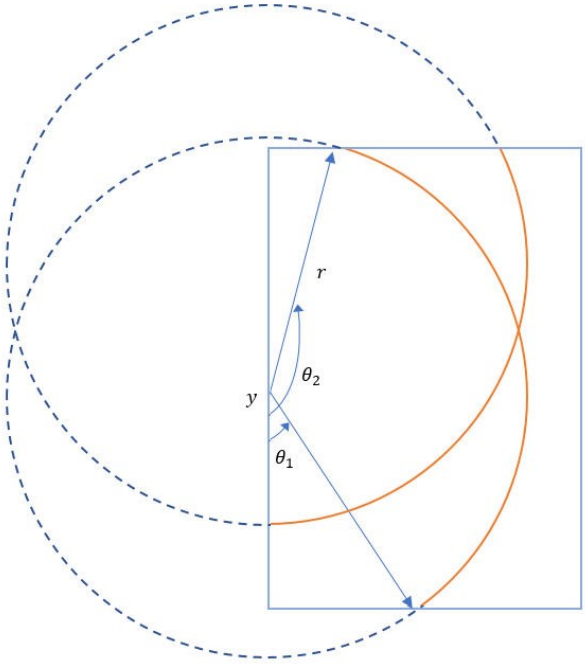

Scheme S3. Notations used in the derivation of the section S1A2.

A3) For $w < r < h$
Two cases are:
1. For $0 < y < h - r$ the arc is from 0 to θ_0, where $\sin(\theta_0) = \frac{w}{r}$, $\theta_0 = \arcsin\left(\frac{w}{r}\right)$
2. For $h - r < y < h - \sqrt{r^2 - w^2}$ the arc is from θ_3 to θ_0, where $\theta_3 = \pi - \theta_2 = \arccos\left(\frac{h-y}{r}\right)$

These two arcs repeat themselves from the other side, so their respective contributions should be multiplied by 2.

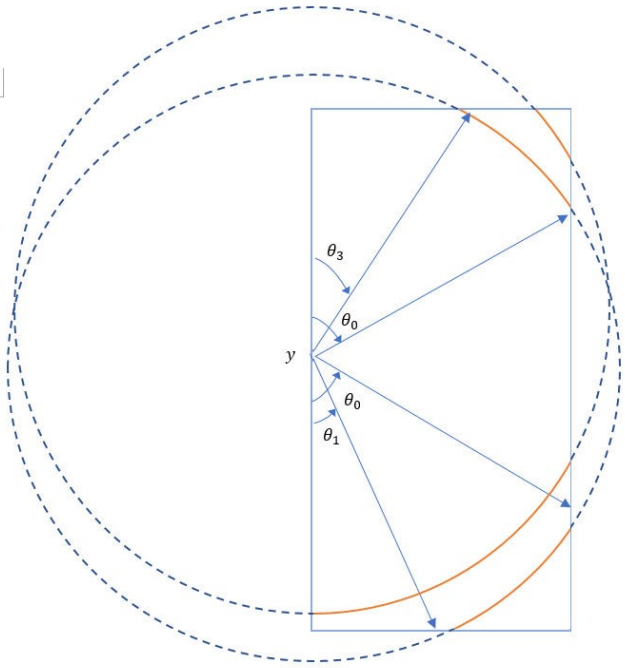

Scheme S4. Notations used in the derivation of the section S1A3.

$$p_{left3}(r) = 2\int_0^{h-r}\left(1 - cos(arcsin\left(\frac{w}{r}\right)\right)dy + 2\int_{h-r}^{h-\sqrt{r^2-w^2}}\left(\frac{h-y}{r} - cos(arcsin\left(\frac{w}{r}\right)\right)dy = \frac{2hr - w^2 - 2h\sqrt{r^2-w^2}}{2\pi r}$$

A4) For $h < r < \sqrt{h^2+w^2}$
Two cases are:
1. For $0 < y < h - \sqrt{r^2-w^2}$ the arc is from θ_3 to θ_0
2. For $\sqrt{r^2-w^2} < y < h$ the arc is from θ_1 to θ_0

$$p_{left4}(r) = \int_0^{h-\sqrt{r^2-w^2}}\left(\frac{h-y}{r} - cos(arcsin\left(\frac{w}{r}\right)\right)dy + \int_{\sqrt{r^2-w^2}}^{h}\left(\frac{y}{r} - cos(arcsin\left(\frac{w}{r}\right)\right)dy = \frac{r^2 - w^2 - 2h\sqrt{r^2-w^2} + h^2}{2\pi r}$$

One can repeat such derivations for the top edge:

A5) For $r < \frac{w}{2}$
Similar to the first case for the left facet:
1. For $0 < x < r$ the arc is from α_1 to π, where $\alpha_1 = \arccos\left(\frac{x}{r}\right)$
2. For $r < x < h - r$ the arc is from 0 to π
3. For $h - r < x < h$ the arc is from 0 to α_2, where $\alpha_2 = \arccos\left(-\frac{w-x}{r}\right)$

$$p_{top1}(r) = \frac{2w - r}{2\pi}$$

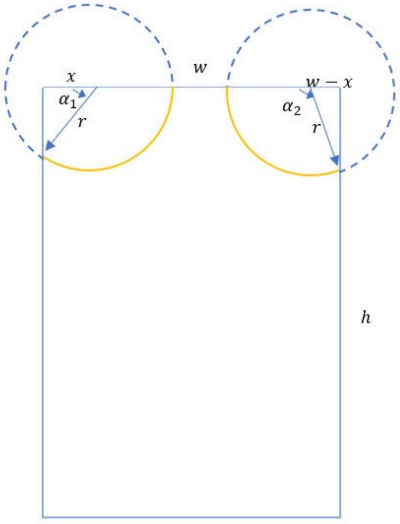

Scheme S5. Notations used in the derivations of the section S1A5.

A6) For $\frac{w}{2} < r < w$
1. For $0 < x < w - r$ countable arc is the same as above: from α_1 to π
2. For $w - r < x < r$ it is from α_1 to α_2
3. For $r < x < w$ it is the same as above: from 0 to α_2

$$p_{top2}(r) = \frac{2w - r}{2\pi}$$

A7) For $w < r < h$ (same range as for left facet)
Only one case needs to be considered:
1. For $0 < x < w$ the countable arc is from α_1 to α_2

$$p_{top3}(r) = \int_0^w \left(\frac{x}{r} + \frac{w-x}{r}\right)dx = \frac{w^2}{2\pi r}$$

A8) For $h < r < \sqrt{h^2+w^2}$
1. For $0 < x < w - \sqrt{r^2-h^2}$ Countable arc is from α_3 to α_0, where $\alpha_0 = \arcsin\left(\frac{h}{r}\right), \alpha_3 = \pi - \alpha_2 = \arccos\left(\frac{w-x}{r}\right)$
2. For $\sqrt{r^2-h^2} < x < w$ Countable arc is from α_1 to α_0

$$p_{top4}(r) = \int_0^{w-\sqrt{r^2-h^2}}\left(\frac{w-x}{r} - cos(arcsin\left(\frac{h}{r}\right)\right)dx + \int_{\sqrt{r^2-h^2}}^{w}\left(\frac{x}{r} - cos(arcsin\left(\frac{h}{r}\right)\right)dx = \frac{r^2 - h^2 - 2w\sqrt{r^2-h^2} + w^2}{2\pi r}$$

Then for the total perimeter of the rectangular (2 left and 2 top edges) a piecewise and continuous function $p(r)$ can be defined as (Figure 1):

$$\begin{cases} p_1(r) = \dfrac{2w + 2h - 2r}{\pi}, & 0 < r < w \\ p_2(r) = \dfrac{2h(r - \sqrt{r^2-w^2})}{\pi r}, & w < r < h \\ p_3(r) = \dfrac{2r^2 - 2h\sqrt{r^2-w^2} - 2w\sqrt{r^2-h^2}}{\pi r}, & h < r < d \end{cases}$$

Normalization coefficient is just the area of the rectangular hw, as would be expected:

$$\int_0^{\sqrt{h^2+w^2}} p(r)dr = \int_0^w p_1(r)dr + \int_w^h p_2(r)dr + \int_h^{\sqrt{h^2+w^2}} p_3(r)dr =$$

$$= \frac{w(w+2h)}{\pi} + \frac{h}{\pi}\left(2h + (\pi-2)w - 2\sqrt{h^2-w^2} - 2w \cdot arctan\left(\frac{w}{\sqrt{h^2-w^2}}\right)\right) + \frac{1}{\pi}\left(2h\sqrt{h^2-w^2} + \pi wh - w^2 - 2h^2 - 2\,hw \cdot arctan\left(\frac{w}{h}\right) - 2hw \cdot arctan\left(\frac{h\sqrt{h^2-w^2} - w^2}{w\sqrt{h^2-w^2} + wh}\right)\right) =$$

$$= \frac{2hw}{\pi}\left(\pi - arctan\left(\frac{w}{h}\right) - arctan\left(\frac{w}{\sqrt{h^2-w^2}}\right) - arctan\left(\frac{h\sqrt{h^2-w^2} - w^2}{w\sqrt{h^2-w^2} + wh}\right)\right) = hw$$

Average value of the distribution:

$$\rho = < r > = \frac{\int_0^{\sqrt{h^2+w^2}} r \cdot p(r)dr}{\int_0^{\sqrt{h^2+w^2}} p(r)dr}$$

First moment (nominator):

$$\frac{1}{3\pi}\left(h^3 + w^3 - (h^2+w^2)^{\frac{3}{2}} + 3hw^2\, ln\left(\frac{\sqrt{h^2+w^2}+h}{w}\right) + 3wh^2\, ln\left(\frac{\sqrt{h^2+w^2}+w}{h}\right)\right)$$

Then the average photon optical path from an isotropic emitter randomly placed in a rectangular:

$$\rho = \frac{1}{3\pi hw}\left(h^3 + w^3 - (h^2+w^2)^{\frac{3}{2}} + 3hw^2\, ln\left(\frac{\sqrt{h^2+w^2}+h}{w}\right) + 3wh^2\, ln\left(\frac{\sqrt{h^2+w^2}+w}{h}\right)\right)$$

For a simple case of a square slab ($h = w = a$):

$$\rho_{sq} = \frac{2\left(1 + 3\, ln\left(1+\sqrt{2}\right) - \sqrt{2}\right)}{3\pi} a \approx 0.47a$$

B) 2D case out-of-plane (XZ plane)

Emitted light from an isotropic emitter reflects many times from the media boundary due to the total internal reflection when the light is emitted outside the escape cone. Individual optical path length between reflections for the light emitted below critical angle θ_{c1} ($\sin(\theta_{c1}) = 1/n$, $\theta_{c1} \approx 42^o$ for $n = 1.5$ of glass or polymers):

$$l_1 = \frac{\Delta}{cos(\theta)}$$

Total optical path in this plane for N bounces until reaching the edge

$$l = N \cdot l_1 = \frac{r}{l_1 \cdot sin(\theta)} \cdot l_1 = \frac{r}{sin(\theta)}$$

where $\theta_{c1} < \theta < \theta_{c2} = \pi - \theta_{c1}$. So l does not deviate much from the distance to the edge r, and is in the range $r < l < nr = \frac{3}{2}r$ (for glass or polymers), depending on the angle θ.

Probability density function for the light emitted from an isotropic emitter is constant $0 < \theta < 2\pi$:

$$g(\theta) = \frac{dP}{d\theta} = \frac{1}{2\pi}$$

Changing variable to the optical path length l for a given parameter r

$$q_r(l) = \frac{dP}{dl} = \frac{dP}{d\theta} \cdot \left|\frac{d\theta}{dl}\right| = g(\theta) \cdot \left|\frac{d\theta}{dl}\right|$$

Where

$$\theta = arcsin\left(\frac{r}{l}\right)$$

Therefore

$$\frac{d\theta}{dl} = -\frac{r}{l\sqrt{l^2-r^2}}$$

Then we obtain

$$q_r(l) = \frac{1}{2\pi} \cdot \frac{r}{l\sqrt{l^2-r^2}}$$

An average value of the optical path from the distribution $q_r(l)$ is close to r:

$$< l > = \frac{\int_r^{3r/2} q_r(l') \cdot l' dl'}{\int_r^{3r/2} q_r(l') dl'} = \frac{2r\left(ln\left(3+\sqrt{5}\right) - ln(2)\right)}{\pi - 2arctan(2/\sqrt{5})} \cdot r = k \cdot r \approx 1.144 \cdot r$$

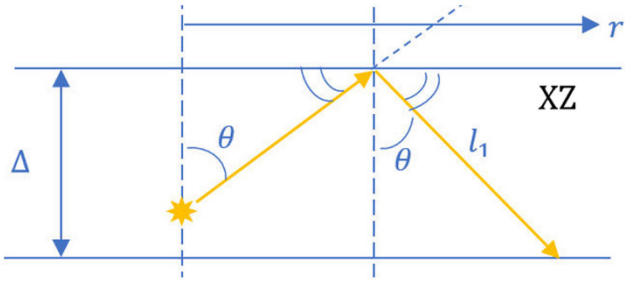

Scheme S6. Notations used in the derivations of the section S1B.

C) 3D case

The distance r from the derived distribution above $q_r(l)$ is not a constant, but has a probability density distribution $p(r)$, where the probability of having $r = r'$ is $p(r')dr'$ for a properly normalized probability density function. That corresponds to the distribution of the optical path lengths:

$$q(l) = \frac{1}{2\pi l}\int_{\frac{2}{3}l}^{l} \frac{p(r')r'}{\sqrt{l^2-r'^2}} dr'$$

Integration limits reflect the fact that only individual distributions with $\frac{2}{3}l < r' < l$ will contribute to the total probability density at the point l. Exact analytical solution is possible to obtain through special functions (complete and incomplete elliptic integrals). Using the following notations:

$$\eta = \frac{\sqrt{l^2 - w^2}}{l}, \varkappa = \sqrt{\frac{4l^2 - 9w^2}{4l^2 - 4w^2}},$$

$$\gamma = \frac{\sqrt{l^2 - h^2}}{l}, \chi = \frac{\sqrt{h^2 + w^2}}{l}$$

One can find that:

For $0 < l < w$

$$q_1(l) = \frac{1}{2\pi l}\int_{\frac{2}{3}l}^{l} \frac{p_1(r')r'}{\sqrt{l^2 - r'^2}}dr'$$

$$q_1(l) = \frac{(12h + 12w - 4l)\sqrt{5} - 9l\left(\pi - 2\,arcsin\left(\frac{2}{3}\right)\right)}{36\pi^2} \approx 0.076(h + w) - 0.068 \cdot l$$

If $w < \frac{2}{3}h$ then for $w < l < \frac{3}{2}w$ (otherwise for $w < l < h$)

$$q_2(l) = \frac{1}{2\pi l}\int_{\frac{2}{3}l}^{w} \frac{p_1(r')r'}{\sqrt{l^2 - r'^2}}dr' + \frac{1}{2\pi l}\int_{w}^{l} \frac{p_2(r')r'}{\sqrt{l^2 - r'^2}}dr'$$

$$q_2(l) = \frac{1}{18\pi^2}\left((6h + 6w - 2l)\sqrt{5} - 9l\left(arcsin\left(\frac{w}{l}\right) - arcsin\left(\frac{2}{3}\right)\right) - 9wk + 18h\left(\frac{w^2}{l^2}K(\eta) - E(\eta)\right)\right)$$

where K, E are complete elliptic integrals of the first and second kind respectively.

If $w < \frac{2}{3}h$ then for $\frac{3}{2}w < l < h$

$$q_3(l) = \frac{1}{2\pi l}\int_{\frac{2}{3}l}^{l} \frac{p_2(r')r'}{\sqrt{l^2 - r'^2}}dr'$$

$$q_3(l) = \frac{1}{\pi^2}\left(\frac{h\sqrt{5}}{3} - hE(\eta) + h\frac{w^2}{l^2}\left(K(\eta) - F(\varkappa, \eta) + \Pi(\varkappa, \eta^2, \eta)\right)\right)$$

where F, Π are incomplete elliptical integrals of the first and third kind respectively.

If $w < \frac{2}{3}h$ then for $h < l < \sqrt{h^2 + w^2}$

$$q_4(l) = \frac{1}{2\pi l}\int_{\frac{2}{3}l}^{h} \frac{p_2(r')r'}{\sqrt{l^2 - r'^2}}dr' + \frac{1}{2\pi l}\int_{h}^{l} \frac{p_3(r')r'}{\sqrt{l^2 - r'^2}}dr'$$

$$q_4(l) = \frac{1}{\pi^2}\left(\frac{h\sqrt{5}}{3} - \frac{h}{2l}\sqrt{l^2 - h^2} + \frac{\pi l}{4} + h\frac{w^2}{l^2}\left(\Pi(\varkappa, \eta^2, \eta) - F(\varkappa, \eta) + K(\eta)\right) - hE(\eta) - wE(\gamma) - \frac{l}{2}arcsin\left(\frac{h}{l}\right) + h^2\frac{w}{l^2}K(\gamma)\right)$$

If $w < \frac{2}{3}h$ then for $\sqrt{h^2 + w^2} < l < \frac{3}{2}h$

$$q_5(l) = \frac{1}{2\pi l}\int_{\frac{2}{3}l}^{h} \frac{p_2(r')r'}{\sqrt{l^2 - r'^2}}dr' + \frac{1}{2\pi l}\int_{h}^{\sqrt{h^2+w^2}} \frac{p_3(r')r'}{\sqrt{l^2 - r'^2}}dr'$$

$$q_5(l) = \frac{1}{\pi^2}\left(arcsin(\chi)\frac{l}{2} - arcsin\left(\frac{h}{l}\right)\frac{l}{2} + h\frac{w^2}{l^2}\left(F\left(\frac{h}{\eta\chi l}, \eta\right) - \Pi\left(\frac{h}{\eta\chi l}, \eta^2, \eta\right) - F(\varkappa, \eta) + \Pi(\varkappa, \eta^2, \eta)\right) + h^2\frac{w}{l^2}\left(F\left(\frac{w}{\eta\chi l}, \gamma\right) - \Pi\left(\frac{w}{\eta\chi l}, \gamma^2, \gamma\right)\right) - \frac{\chi}{2}\sqrt{l^2 - h^2 - w^2} - \frac{h}{2l}\sqrt{l^2 - h^2}\right)$$

To verify these formulas several millions of path lengths were numerically calculated for a point with a varying location inside a 3D slab with given side lengths. Resulting distributions (dots) indeed converge to the analytical expressions presented here (blue and red lines).

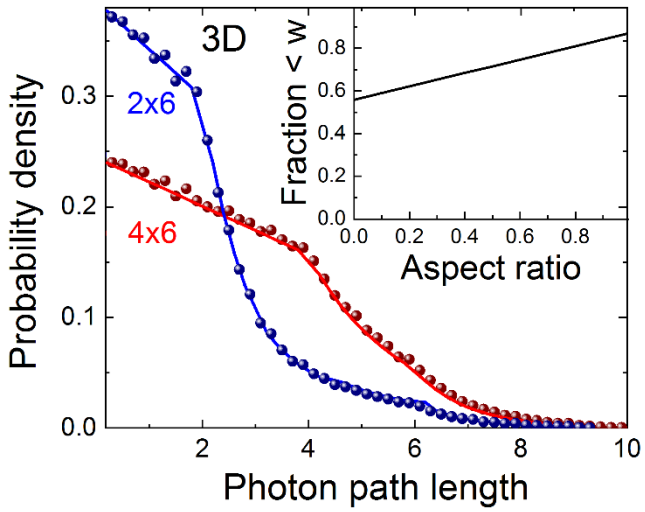

Figure S1. Probability density function distributions for a 3D slab with dimension 2x6 (blue) and 4x6 (red) units. Points are counted by simulating about a million paths from an isotropic emitter, and solid lines are analytical solutions from above. Inset shows fraction of optical paths below the width w of a rectangular (aspect ratio $\beta = w/h$).

Section S2. Approximate solution for the optical path distribution

A) Derivation of the approximate solution

The exact solution presented above is not very convenient to work with, so an approximate analytical solution would be easier to use instead. It can be obtained based on the fact that $q_r(l)$ varies only marginally, being chiefly close to r. So, as a first approximation, one can substitute distribution $q_r(l)$ by its average value $l \approx < l >= k \cdot r$ and to rely solely on the obtained 2D distribution $p(r)$. So the approximate analytical distribution for the optical path length distribution in 3D can be written as

$$\boldsymbol{q(l) \approx p(l/k)}$$

It appears to be a very good approximation for different aspect ratio geometries (Figure 1, inset). The meaning of the coefficient $k \approx 1.14$ can be then interpreted as a correction for 3D geometry from a 2D case. So the final solution $q'(l)$ becomes:

$$\begin{cases} \dfrac{2w+2h-2l/k}{\pi}, & 0 < l < kw \\ \dfrac{2h(l-\sqrt{l^2-(kw)^2})}{\pi l}, & kw < l < kh \\ \dfrac{2l^2/k-2h\sqrt{l^2-(kw)^2}-2w\sqrt{l^2-(kh)^2}}{\pi l}, & kh < l < kd \end{cases}$$

Using normalization coefficient:

$$\int_0^{k\sqrt{h^2+w^2}} q'(l)dl = k \cdot \int_0^{\sqrt{h^2+w^2}} p(r)dr = khw$$

A properly normalized 3D probability density function $q(l)$ then becomes:

$$\begin{cases} \dfrac{2w+2h-2l/k}{\pi hwk}, & 0 < l < kw \\ \dfrac{2l-2\sqrt{l^2-(kw)^2}}{\pi lwk}, & kw < l < kh \\ \dfrac{2l^2/k-2h\sqrt{l^2-(kw)^2}-2w\sqrt{l^2-(kh)^2}}{\pi lhwk}, & kh < l < kd \end{cases}$$

B) Probability of the optical path to be shorter than the rectangular width

The probability for an optical path to be shorter than the rectangular width w (aspect ratio $\beta = \frac{w}{h} \leq 1$):

$$P_w = \int_0^w q(l)dl = \frac{2}{k\pi}\left(\beta + 1 - \frac{\beta}{2k}\right) \approx 0.31\beta + 0.56$$

It is shown in the inset of Figure S1 as a function of β. So most of the photon path distribution lies below the shortest side of the rectangular. Even for a very large 1:5 ratio it is > 60% probability, reaching ~ 85% for the squared shape. For the "golden ratio" $\frac{2}{1+\sqrt{5}} \approx 0.62$ it is 75%. So for most practical applications it is possible to say that the rectangular width mainly limits optical path of photons in a 3D slab.

Section S3. Effect of matrix absorption

The probability of having optical path $l = l'$ is $q(l')dl'$ for a properly normalized probability density function $q(l)$. Then

$$f(\alpha) = \int_0^{lmax} q(l') \cdot exp(-\alpha l')dl'$$

Which essentially shows the fraction of photons reaching the edge for given h and w (diagonal $d = \sqrt{h^2+w^2}$) of a rectangular, where $l_{max} = kd$. Calculating dimensionless $f(\alpha)$ using obtain normalized distribution $q(l)$ yields:

$$f_1(\alpha) = \int_0^{kw} q_1(l') \cdot exp(-\alpha l')dl' = \frac{2}{\alpha^2 hw\pi k^2}\left((h+w)\alpha k - 1 + e^{-kw\alpha}(1 - kh\alpha)\right)$$

$$f_2(\alpha) = \int_{kw}^{kh} q_2(l') \cdot exp(-\alpha l')\, dl' = \frac{2}{\alpha w\pi k}\left(e^{-kw\alpha} - e^{-kh\alpha}\right) - \frac{2}{w\pi k}\int_{kw}^{kh} \frac{\sqrt{l^2-(kw)^2}}{l} exp(-\alpha l)dl$$

$$f_3(\alpha) = \int_{kh}^{kd} q_3(l') \cdot exp(-\alpha l')\, dl' = \frac{2}{\alpha^2 hw\pi k^2}(\alpha hk \cdot e^{-\alpha hk} - d\alpha k \cdot e^{-\alpha dk} + e^{-\alpha hk} - e^{-\alpha dk}) - \frac{2}{w\pi k}\int_{kh}^{kd} \frac{\sqrt{l^2-(kw)^2}}{l} exp(-\alpha l)\, dl - \frac{2}{h\pi k}\int_{kh}^{kd} \frac{\sqrt{l^2-(kh)^2}}{l} exp(-\alpha l)dl$$

$$f(\alpha) = f_1(\alpha) + f_2(\alpha) + f_3(\alpha)$$

$$f(\alpha) = \frac{2}{\alpha^2 hw\pi k^2}\left((h+w)\alpha k - (kd\alpha + 1) \cdot e^{-kd\alpha} + e^{-kh\alpha} + e^{-kw\alpha} - 1\right) - \mathfrak{I}_1 - \mathfrak{I}_2$$

where two integrals are:

$$\mathfrak{I}_1 = \frac{2}{w\pi k}\int_{kw}^{kd} \frac{\sqrt{l^2-(kw)^2}}{l} exp(-\alpha l)\, dl,$$

$$\mathfrak{I}_2 = \frac{2}{h\pi k}\int_{kh}^{kd} \frac{\sqrt{l^2-(kh)^2}}{l} exp(-\alpha l)dl$$

Section S4. Fraction of light emitted to the waveguiding mode

The emitted light from a fluorophore (quantum dot, organic dye, etc.) in a polymer/glass slab will experience total internal reflection for angles at the air interface larger than a critical angle α_c. In the most common case for a glass or a polymer: $n = 1.5$, $n_{air} = 1$ and the critical angle α_c:

$$sin(\alpha_c) = \frac{1}{n}$$

i.e. $\alpha_c \approx 42°$. Thus, for the emitter in a rectangular slab with six facets there are six cones with the angle $2\alpha_c$, where the emitted light can escape. Solid angle of the cone (surface of a spherical cap) for a unity radius sphere is

$$S_1 = 2\pi(1 - cos\, \alpha_c)$$

So the fraction of the emitted light through one facet is:

$$\delta_1 = \frac{S_1}{S} = \frac{2\pi(1 - \cos\alpha_c)}{4\pi} = \frac{\left(1 - \frac{\sqrt{n^2-1}}{n}\right)}{2}$$

Considering only emitted light through top and bottom facets as losses the total useful fraction of the emission is then ($n = 1.5$):

$$\delta = 1 - 2\delta_1 = \frac{\sqrt{n^2-1}}{n} \approx 75\%$$

Section S5. Effect of scattering by fluorophores

If the total loss is governed by the scattering instead (absorption-free matrix and re-absorption free fluorophore) then the optical efficiency can be also evaluated from the optical path length distribution. Let the linear scattering coefficient be $\alpha_{sc}[1/cm]$. Probability for the photon to travel optical path l' before reaching the edge is $q(l')dl'$. Probability of not being scattered within distance l' is $\exp(-\alpha_{sc}l')$. These photons will contribute to the total optical efficiency similarly to the absorption case above:

$$\chi_0(\alpha_{sc}) = \int_0^{lmax} q(l') \cdot exp(-\alpha_{sc}l')\, dl' = f(\alpha_{sc})$$

In addition, there will be photons, which underwent scattering into the waveguiding mode. Probability of being scattered within distance l' is $1 - \exp(-\alpha_{sc}l')$. If δ is a fraction of waveguided light after a scattering event (δ=75% for n=1.5) the probability to reach the edge after one scattering event is:

$$\chi_1(\alpha_{sc}) = \delta \cdot \int_0^{lmax} q(l') \cdot (1 - exp(-\alpha_{sc}l'))dl' \cdot \int_0^{lmax} q(l') \cdot exp(-\alpha_{sc}l')\, dl'$$

$$\chi_1(\alpha_{sc}) = \delta \cdot (1 - f(\alpha_{sc})) \cdot f(\alpha_{sc})$$

A Markov process is considered, where there is no memory in the system. The total probability for a photon to reach the edge becomes then a geometrical series (sum of probabilities for no scattering, one scattering, two scattering events, etc.):

$$\chi(\alpha_{sc}) = \sum_{i=0}^{\infty} \chi_i = f(\alpha_{sc})\left[1 + \delta \cdot \left(1 - f(\alpha_{sc})\right) + \left(\delta \cdot \left(1 - f(\alpha_{sc})\right)\right)^2 + \ldots\right] = \frac{f(\alpha_{sc})}{1 - \delta \cdot \left(1 - f(\alpha_{sc})\right)}$$

Section S6. Effect of several loss mechanisms present simultaneously

Now consider two processes taking place simultaneously: scattering and matrix absorption. First, photons experiencing no scattering and no absorption will contribute to the total signal:

$$\psi_0(\alpha_{sc}, \alpha) = \int_0^{lmax} q(l') \cdot \exp(-\alpha_{sc}l') \cdot \exp(-\alpha l')\, dl' = f(\alpha_{sc} + \alpha)$$

Then photons after one scattering event and without subsequent scattering and absorption. While every scattering event sets back to zero the travelled distance for scattering, the optical path for absorption continues. So the exact history of scattering becomes important. To take into account this fact one can introduce a probability *density* to scatter at a point l' (in the absence of other processes):

$$p_{sc}(l') = \alpha_{sc} \cdot exp(-\alpha_{sc}l')$$

which is a properly normalized probability density function. Then in the system where scattering and absorption coexist the probability density to scatter at a point l' without being absorbed before is:

$$p_{sc}(l') \int_{l'}^{\infty} p_{ab}(x)dx$$

where a similar notation of the probability density p_{ab} is introduced for the pure absorption process. Additional conditions of no subsequent scattering and absorption can be added as:

$$p_{sc}(l') \int_{l'}^{\infty} p_{ab}(x)dx \cdot \delta \cdot exp(-\alpha_{sc}l_2) \cdot exp(-\alpha l_2)$$

where l_2 is a photon path taken to reach the device edge after the scattering event. If l' varies in between $(0; l_1)$ the integrated *probability* becomes:

$$\delta\, exp(-(\alpha_{sc} + \alpha)l_2) \int_0^{l_1} \alpha_{sc}\, exp(-\alpha_{sc}l')\, exp(-\alpha l')\, dl' = exp(-(\alpha_{sc} + \alpha)l_2) \frac{\delta\alpha_{sc}}{\alpha_{sc} + \alpha}[1 - exp(-(\alpha_{sc} + \alpha)l_1)]$$

Finally taking into account probability to have photon path l_1 as $q(l_1)dl_1$ and l_2 as $q(l_2)dl_2$ (again Markov process without memory in the system considered) one obtains after integration from zero to l_{max} for both path stretches $l_{1,2}$ the input from the photons experienced one scattering event:

$$\psi_1(\alpha_{sc}, \alpha) = f(\alpha_{sc} + \alpha) \cdot \delta\alpha_{sc} \frac{[1 - f(\alpha_{sc} + \alpha)]}{\alpha_{sc} + \alpha}$$

Continuing in the same manner for two scattering events without subsequent scattering and absorption:

$$\psi_2(\alpha_{sc}, \alpha) = f(\alpha_{sc} + \alpha) \cdot (\delta\alpha_{sc})^2 \left(\frac{[1 - f(\alpha_{sc} + \alpha)]}{\alpha_{sc} + \alpha}\right)^2$$

So the resulting probability can be again represented through geometrical series:

$$\psi(\alpha_{sc}, \alpha) = \sum_{i=0}^{\infty} \psi_i(\alpha_{sc}, \alpha) = \frac{f(\alpha_{sc} + \alpha)}{1 - \delta \cdot \frac{\alpha_{sc}}{\alpha_{sc} + \alpha} \cdot [1 - f(\alpha_{sc} + \alpha)]}$$

This formula turns into the expression for scattering only scenario for a non-absorbing matrix ($\alpha = 0$). A similar result can be derived for the case of re-absorption instead of scattering:

$$\boldsymbol{\phi(\alpha_{re}, \alpha)} = \frac{\boldsymbol{f(\alpha_{re} + \alpha)}}{\boldsymbol{1 - \delta \cdot QY \cdot \frac{\alpha_{re}}{\alpha_{re} + \alpha} \cdot [1 - f(\alpha_{re} + \alpha)]}}$$

When re-absorption and scattering both exist in the system one can show in a similar manner as above:

$$\boldsymbol{\varphi(\alpha_{sc}, \alpha_{re})} = \frac{\boldsymbol{f(\alpha_{sc} + \alpha_{re})}}{\boldsymbol{1 - \frac{\delta \cdot \alpha_{sc} + \delta \cdot QY \cdot \alpha_{re}}{\alpha_{sc} + \alpha_{re}} \left(1 - f(\alpha_{sc} + \alpha_{re})\right)}}$$

A general solution for the optical efficiency $g(\alpha_{sc}, \alpha_{re}, \alpha)$, following derivations above, is:

$$\boldsymbol{g} = \frac{\boldsymbol{f(\alpha_{sc} + \alpha_{re} + \alpha)}}{\boldsymbol{1 - \frac{\delta \cdot \alpha_{sc} + \delta \cdot QY \cdot \alpha_{re}}{\alpha_{sc} + \alpha_{re} + \alpha} \left(1 - f(\alpha_{sc} + \alpha_{re} + \alpha)\right)}}$$